Spatially-resolved current and impedance analysis of a stirred tank reactor and serpentine fuel cell flow-field at low relative humidity

Warren H.J. Hogarth [a,*], Johannes Steiner [b], Jay B. Benziger [c], Alex Hakenjos [b]

[a] *ARC Centre for Functional Nanomaterials, The University of Queensland, Australia*
[b] *Fraunhofer Institute for Solar Energy Systems ISE, Freiburg, Germany*
[c] *Department of Chemical Engineering, Princeton University, NJ, USA*

Abstract

A 20 cm^2 segmented anode fuel cell is used to investigate the performance of a hydrogen-air fuel cell at 1 atm. with two different flow-fields using spatially-resolved current and impedance measurements. A self-draining stirred tank reactor (STR) fuel cell and a single-channel serpentine fuel cell are compared with humidified and dry feed conditions. The current density distribution, impedance distribution, heat distribution and water evolution are compared for the two different flow-fields. With inlet feed dew points of 30 °C, the STR fuel cell and serpentine system performed comparably with moderate current gradients. With drier feeds, however, the STR fuel cell exhibited superior overall performance in terms of a higher total current and lower current, impedance and temperature distribution gradients. The STR fuel cell design is superior to a single-channel serpentine design under dry conditions because its open channel design allows the feed gases to mix with the product water and auto-humidify the cell.
© 2006 Elsevier B.V. All rights reserved.

Keywords: Stirred tank reactor fuel cell; Current density distribution; Impedance; Auto-humidification; Spatially-resolved impedance; Single-channel serpentine design

1. Introduction

Proton-exchange membrane fuel cells (PEMFCs) are being investigated as alternatives to traditional power-generation technology in off-grid power and transportation applications. For such applications, it is essential that these systems are capable of running under standard atmospheric conditions. Present PEMFC technology is optimized to run with feed streams of hydrogen and air at between 1 and 3 atm. and 60–80 °C and close to 100% relative humidity (RH) [1,2], whereas typical environmental conditions are 1 atm. −20–40 °C with a maximum dew point of ∼30 °C. To simplify design and make a robust and versatile system capable of being deployed 'anywhere', it is necessary to develop systems that can operate under these harsh conditions.

To address the humidification problem, manufacturers typically integrate humidification systems into the system design.

This adds unnecessary weight and volume to the system and often requires that water be carried on-board. One solution to this problem that has been trialled at Fraunhofer ISE, is to integrate the membrane humidification process into the stack itself [3]. This has proved successful in the systems tested to date. An alternative has been the STR fuel cell design which uses the water produced internal to the fuel cell to auto-humidify the cell and thus removes the need for any pre-treatment of the feed streams [4].

The STR concept developed by the Benziger group [5] was designed by considering how flow-field design could be best optimized for dry-feed operation. The basic principle of the design is that the tortuous long flow path of the serpentine system, which has high gas velocities, is replaced by an open flow channel system with low gas velocity. By significantly reducing the gas velocity, diffusion of the gases becomes the dominant transport mechanism. By allowing diffusive back-mixing in the system, water that is produced internally in the cell can humidify the entire reaction chamber.

Recently, Hogarth and Benziger [4] showed that the STRFC can operate at up to 115 °C at 3 atm. with dry feeds of hydrogen

* Corresponding author. Tel.: +617 3365 3885; fax: +617 3365 6074.
E-mail address: warrenhogarth@hotmail.com (W.H.J. Hogarth).

and oxygen or air. The authors characterized the STR system by developing design equations to describe the operating temperature and pressure ranges with oxygen or air flows at the cathode. They successfully demonstrated that the performance of a dry-feed STR fuel cell was similar to a serpentine system with fully humidified feeds. Additionally, the dynamic operation of the system has been investigated to characterize ignition and extinction phenomena, detect the presence of multiple steady-states, and demonstrate a simple direct injection ignition system [6]. As a result of the investigation, an optimum operation regime defining the performance envelop as a function of flow rates, temperature, pressure and external load has been developed.

In this Study, the design was adopted to the test cell developed by Hakenjos et al. [7]. This cell, together with the measurement equipment, allows for spatially-resolved current and impedance analysis. Measurements under a series of simulated atmospheric operating conditions were compared with those obtained for a single channel serpentine system. The aim was to develop scale-up of the technology for small off-grid systems and prove that the superior performance of the STR system at low RH is a result of back diffusion which allows the system to auto-humidify.

2. Experimental

2.1. Segmented anode fuel cell

The previously reported segmented PEM fuel cell with an active area of $20\,cm^2$ was used for all experiments [7,8]. Briefly, the anode of the fuel cell was segmented into 7×7 square current-collectors which were equally distributed over the anode (Fig. 1). Each current-collector was connected with a separate current line and voltage sensor. These were connected back to a 50 channel potentistat and a Solartron 1254 frequency response analyser (FRA) with two 1251 multi-channel extensions to provide a total of 19 channels for the FRA. All current and impedance measurements were taken with the local potential of each segment set at 0.4 V to prevent any cross currents in

Fig. 1. Photograph of segmented anode flow field showing current-collectors and optical and infra-red viewing window.

the electrode. Current density distributions were generated by measuring the local current of each segment after equilibrating the fuel cell for an extended period of up to 4 h. The impedance was calculated using the absolute value at 1 kHz, as previously described [8]. Changes in the impedance throughout a single test were assumed to be due to a change in the ionic resistivity of the membrane which is caused by a change in hydration.

2.2. Testing conditions

Flow rates of hydrogen and air, temperature and dew points of the feed streams were controlled. The streams were humidified by passing dry air through temperature-controlled bubblers. The dew points of the streams were measured using dew point mirrors and controlled by mixing appropriate amounts of humidified and dry feed gas. The inlet feed lines were heated to 40 °C to prevent any condensation of liquid water. Exit gas dew points, the cell temperature, the clamping pressure of the cell and individual segment currents were monitored. There was no heat input into the cell and no temperature control was imposed on the cell, rather the temperature was monitored for gradients. The temperature was a function of the total current, flow rates and water content of the flow streams. The cathode of the fuel cell was fitted with a zinc selenide window to allow both optical and infra-red observations of behaviour. A JENOPTIK 3021-ST high resolution IR camera was used to obtain temperature distributions at the cathode. The system was calibrated as previously described [7]. All tests were performed with $25\,\mu m$ Gore Primea 5510 membrane electrode assemblies (MEAs) with $0.4\,mg\,cm^{-2}$ of Pt catalyst and a carbon paper gas-diffusion layer (GDL) with a microporous layer and wet proofing. The latter was obtained from the SGL Carbon Group, Germany.

2.3. Cathode flow-field design

Two cathode flow-fields were investigated: a STR fuel cell and a standard single-channel serpentine system. The STR fuel cell design is shown in Fig. 2(a). It is orientated as a diamond. Gas enters at the top and leaves at the base. Current-collectors are evenly distributed throughout the cell and align with the segments at the anode. The design allows water that is formed to self drain due to gravity and surface tension causes it to bead on the outside of the GDL. To satisfy the design criteria and to scale-up from 1.9 to $20\,cm^2$, alterations had to be made to the gas manifold, namely, it was extended along the top two to edges of the cell. This was to ensure that the inlet gas velocity was low, that the gas was well distributed, and that the mean free path of the gas was reduced. It is believed that the combination of these three factors should allow the well-mixed nature that is the fundamental basis of the cell design to be satisfied on scale-up.

The MEA side of the STR flow channel is shown in Fig. 2(b). The open design and current-collectors are clearly visible. There are two different cut-away depths around the flow channels at 1.5 and 3 mm. Normally, there would only be one single cut-away depth, but to allow optical and thermographic analysis of the cathode, half of the flow area was cut right through the
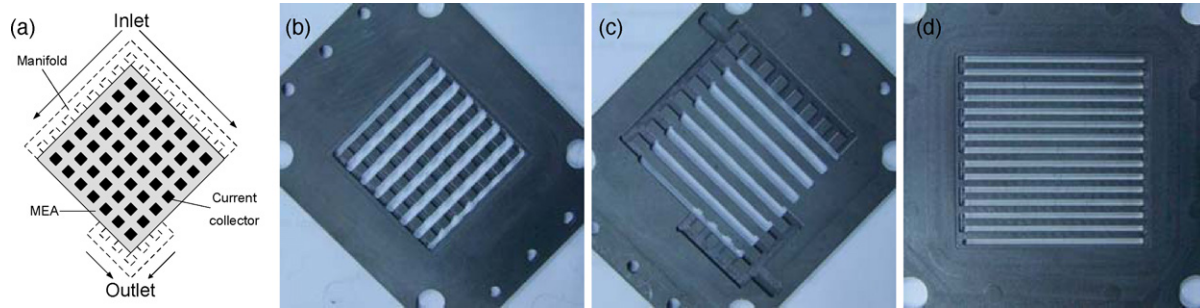
Fig. 2. Cathode flow field design: (a) schematic of 20 cm² STR cathode flow-field; (b) photograph of MEA side of STR flow-field; (c) photograph of gas manifold side of STR fuel cell; (d) photograph of single-channel serpentine flow field.

carbon. The gas manifold cut into the reverse side of the carbon plate, is illustrated in Fig. 2(c) and the serpentine flow channel system in Fig. 2(d). Similar to the STR design, a portion of the flow channels are cut all the way through the carbon to allow thermographic and optical analysis of the cathode.

3. Results

The STR fuel cell was operated under the conditions reported in Table 1. Three standard inlet flow conditions were tested, namely:

(i) a dew point of 30 °C was chosen to represent best case atmospheric conditions
(ii) a dew point of 10 °C to represent moderate conditions
(iii) dry feeds to represent a worst case scenario.

The average current and temperature at 0.4 V of each flow geometry tested under the alternate operating conditions are shown in Table 1, together with the maximum cell temperature recorded by the infra-red camera and the calculated exit RH of the system. The exit RH was calculated at the maximum fuel cell temperature using a mass balance on the system. Water partitioning caused by the membrane was neglected for simplicity and hence the calculated RH represents a weighted average for both the air and hydrogen exit gas streams.

The data given in Table 1 clearly show that the STR fuel cell outperformed the serpentine design under all scenarios. Under the best case conditions with dew points at 30 °C, the STR design was 5–10% better, but under dry conditions where the STR

is specifically designed to operate, the advantage increased to almost 25% when measured in terms of current density ignoring cell temperature effects. It is important to note that while the overall current densities may seem low, the system is not optimized for performance—the cell uses steel electrodes for the segmented anode and this increases the contact resistance, the system is only at 1 atm., and the RH is below 100%. The aim is to compare the two alternative flow channel designs at the same conditions.

The average current density is presented in Fig. 3 as a function of time for the STR fuel cell and the serpentine fuel cell.
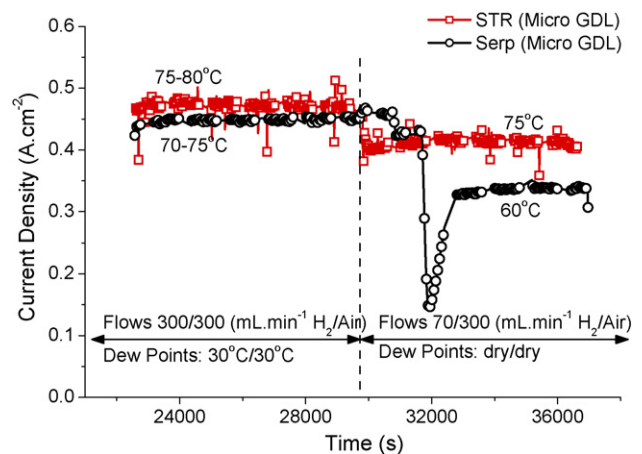

Fig. 3. STR and serpentine segmented fuel cell current density operating at 0.4 V with dew points of 30 °C and dry air feeds. Hydrogen flow rate adjusted down under dry conditions to reduce water convection from fuel cell.

Table 1
Fuel cell operating conditions, maximum fuel cell temperature and calculated outlet RH of exit streams for STR and serpentine fuel cells

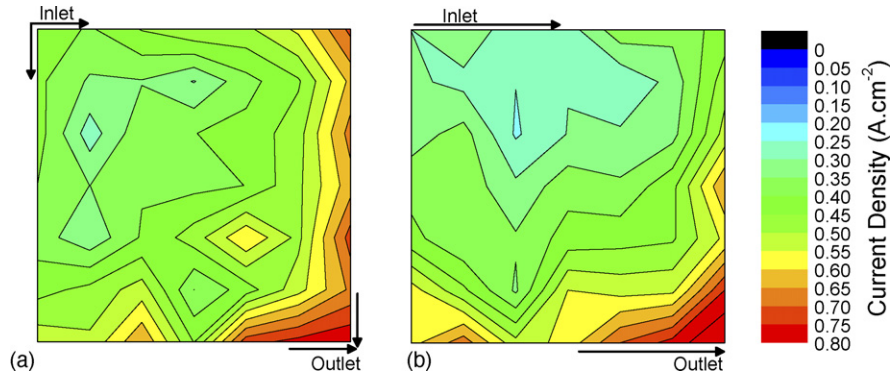| Flow design	Dew point H₂/Air (°C)	Flow rate H₂/Air (mL min⁻¹)	Stoich H₂/Air	Current (A cm⁻²)	Max cell temp. (°C)	Outlet RH @ max cell temp. (%)
STR	30/30	108/454	1.6/2.7	0.48	85	34
	10/10	108/454	1.8/3.0	0.43	80	30
	Dry/dry	70/300	1.2/2.1	0.42	75	54
	30/30	300/300	4.6/1.8	0.47	80	39
Serpentine	30/30	108/454	1.8/3.0	0.43	75	46
	10/10	108/454	2.0/3.3	0.39	75	33
	Dry/dry	70/300	1.5/2.5	0.34	60	80
	30/30	300/300	4.8/1.9	0.45	75	46

Fig. 4. Spatially-resolved current density distribution in (a) STR fuel cell and (b) serpentine fuel cell under 'best case' scenario with 30 °C dew points and flow rates of 108 and 454 mL min⁻¹ for hydrogen and air, respectively.

The voltage of each individual segment was set at 0.4 V and the conditions are marked on the graph. Under the best case scenario with dew points of 30 °C, the STR fuel cell performs only marginally better than the serpentine system. When the feed is changed to dry streams, the performance of the STR fuel cell is improved significantly. It is important to note that the STR fuel cell performs better even though it is operating at a higher temperature. As the current density of the system increases, the cell temperature increases. The latter will rise the saturated vapour pressure exponentially, negating any linear increase in the RH in the cell caused by the greater water production.

The results in Fig. 3 also provide an insight into the effect on the system caused by a disturbance in the two flow regimes. When the flow rates are changed from the humidified regime to dry feed there is only a 10% fall in performance for the STR fuel cell, i.e., from 0.47 to 0.42 A cm⁻², whereas for the serpentine fuel cell there is a significantly greater drop in performance of 30%. Additionally, Fig. 3 shows that there is also a lag in the performance of the serpentine system, followed by a rapid drop in current before the cell recovers. When observing the change in current density distribution and temperature profiles for this period (not shown) it is apparent that the membrane goes through a dehydration stage and this causes the lag. After this period, the performance drops rapidly and only recovers as the cell cools, which lowers the saturated vapour pressure of the water and hence increases the RH.

Figs. 4 and 5 show the experimentally determined spatially-resolved current density for the STR fuel cell and the serpentine fuel cell with feed inlet dew points of 30 °C and with dry feeds, respectively. For all STR graphs, the feed entry was along the left and top sides of the graphs and exited in the lower right corner, as indicated. The STR graphs would need to be rotated 45° clockwise to orientate them in the exact same configuration as the fuel cell was operated (Fig. 2(a)–(c)). In the serpentine system, the feed entered at the top left and snaked its way to the lower right in 7.5 turns, as indicated by Fig. 2(d). The serpentine system was orientated in the same position as the graph.

A comparison of the current density for the STR fuel cell and the serpentine fuel cell operating under the 'best case' scenario with inlet dew points of 30 °C is given in Fig. 4. In both cases, the majority of the cell operated between 0.30 and 0.50 A cm⁻² with the STR design appearing to be slightly more uniform. Both flow designs also have a large increase in the current density near the outlet of the cell.

The current densities of the two cell designs under the extreme conditions with dry feed streams are presented in Fig. 5. Under these harsh conditions the advantage of the STR fuel cell becomes clear. In the serpentine system, there is a large dead zone in the first third of the cell where the current is <0.05 A cm⁻². After the dead zone, the current density then changes rapidly with a steep gradient. Meanwhile, the STR fuel cell has significantly reduced entrance effects, so that a greater
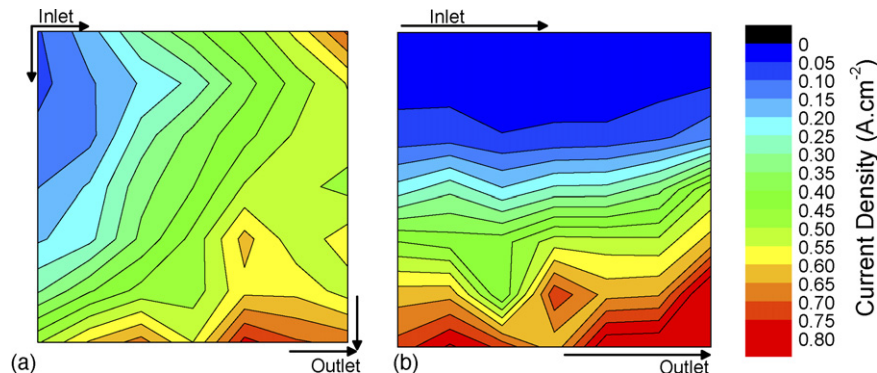

Fig. 5. Spatially-resolved current density distribution in (a) STR fuel cell and (b) serpentine fuel cell under the 'worst case' scenario with dry feed streams and flow rates of 70 and 300 mL min⁻¹ for hydrogen and air, respectively.
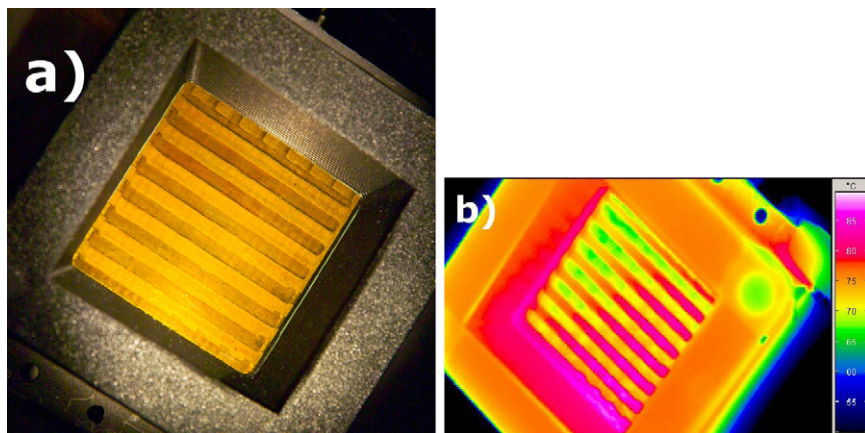
Fig. 6. (a) Optical photograph and (b) infra red photograph STR fuel cell operating with dry feeds 70 and 300 mL min^{-1} of hydrogen and air, respectively.

area of the fuel cell is utilized. As a result, the overall performance of the STR fuel cell is higher and the gradients, indicated by the spacing of the contour lines, are significantly less steep. The entrance effects are diminished because the design allows for appreciably more diffusive back-mixing.

The current density plots (not shown) of the two flow channel designs under the mild conditions with inlet feed dew points of 10 °C are similar to the dry feed plots, except that the entrance effects and gradients in both cells are less severe. The STR fuel cell displays superior overall performance with lower gradients, but the advantage is not as significant as under the extreme conditions.

An optical photograph of the STR fuel cell operating under the worst case conditions with dry feeds, is shown is Fig. 6(a). Only half the channels could be cut through the graphite so as not to disrupt the conduction pathways of the current-collectors. Throughout the tests, no liquid water could be seen evolving from the GDL and the flow channels were completely dry. Even when running under best case conditions, no flooding was evident. The only time liquid water droplets were observed in the cell was when the fuel cell was operated with the gas feed streams starved (stoichiometry <1.0). Under starvation conditions, there was not enough gas leaving the cell to remove the water as a vapour and hence liquid water formed. When liquid water droplets were observed, they would bead on the outside of the GDL and immediately run down under gravity to the exit at the base of the cell. The water droplets bead on the outside of the GDL because it is hydrophobic. This process is facilitated in the STR design because the pathway of the water droplets to the exit is unimpeded as compared with a tortuous serpentine system. Occasionally under starvation conditions there was evidence of a build-up in liquid water at the base of the cell. It is thought that this was because the exit pipes were too small for the water to self drain.

The temperature profile in the STR fuel cell operating under the worst case scenario with dry feeds is shown in Fig. 6(b). The inlet gas, which was preheated to 40 °C, enters the flow chamber and is mixed with gas in the chamber. The gas in this mixing zone is at approximately 65 °C and represents the first quarter

of the total chamber. By the time the gas reaches the lower half of the chamber it has been heated to about 75 °C. In the lower half of the chamber the gas temperature is roughly constant. The external clamps, etc. of the cell (the black area around the flow chamber in Fig. 6(a) are at 75 °C. Parts of the graphite electrode that are not cut-away experience temperatures of up to 85 °C.

The results of the spatially-resolved impedance analysis on the STR fuel cell when operated under the worst case conditions with dry feeds are presented in Fig. 7. These measurements were taken immediately before the current density distribution in Fig. 5(a). The resolution of the impedance distribution is not as high as the current distribution, as these was capacity for only a 4 × 4 array. Despite this, it is clear that the impedance data corroborated the current density distribution data given the assumption that a low conductivity is the result of a high membrane resistance. The resistance is highest at the upper left quarter of the cell where the majority of the gas enters the cell. Outside this zone, the resistance is significantly lower and the lowest point is at the exit in the lower right corner.
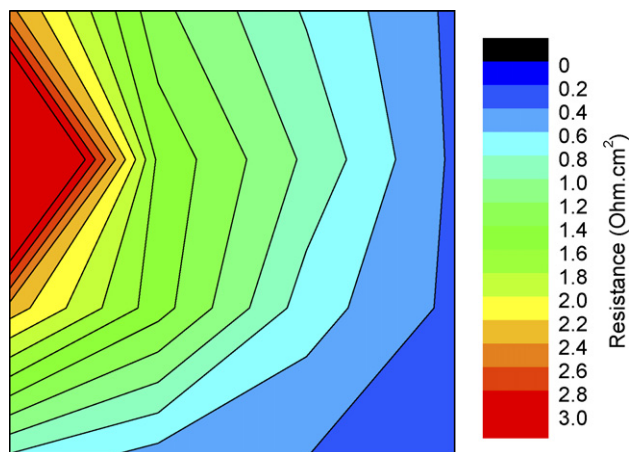

Fig. 7. Spatially-resolved impedance analysis of STR fuel cell operating with dry feeds of 70 and 300 mL min^{-1} of hydrogen and air, respectively. Impedance measurements taken immediately before current density distribution in Fig. 5(a).

4. Discussion

The performance of the STR fuel cell is superior to that of the single-channel serpentine fuel cell when operated with dry and partially humidified feeds, namely:

 (i) the STR design has higher current densities for all tested conditions;
 (ii) the current density with the STR design is more uniform under all tested conditions, which implies better MEA utilization especially with dry feeds;
(iii) the STR cell performance is not adversely affected by changes in the dew point of the feed streams, while the total current decreases significantly with serpentine flow channels.

The superior performance of the STR fuel cell when operated with non-saturated feed streams is due to the flow-field design. The key to optimizing dry feed performance of a fuel cell is to make best use of the water that is produced internally to humidify as much of the fuel cell as possible. There are two key methods to optimize water management, as follows:

 (i) Reduce the amount of water that is convected down stream in the fuel cell flow-channels. If water is convected down stream, it cannot be used to humidify the inlet gas stream. Convection can be optimized using control parameters to slow excess gas flow rates, design parameters to increase the cross-sectional area of flow channels, or parallel-flow channels [4].
 (ii) Optimize the design of the flow-field to promote back diffusion. Invariably when operating non-saturated feed fuel cells, the partial pressure of water (RH), will be lowest at the entrance and highest at the exit. This effect is clearly evident in Fig. 5. Therefore, if diffusion in the fuel cell can be optimized, a molecule of water formed towards the exit

can diffuse further towards the entrance. This increases the humidity of the cell at the entrance, reduces concentration gradients, and increases overall performance.

A single-channel serpentine fuel cell is not optimized to maximize diffusion. Generally, serpentine fuel cells have a single, long tortuous channel with a very small cross-sectional area. Consequently, the velocity of the gas in the flow stream is extremely high, and the mean free path for a molecule to diffuse from the exit to the entrance is maximized. Such conditions minimize back-diffusion and are representative of a plug flow reactor. Because water cannot back-diffuse easily in the cell, the gas at the entrance cannot easily humidify. This is why there is a large dead zone at the entrance of the fuel cell in Fig. 5(b). Once the stream begins to humidify, any water that is produced is convected down-stream due to the high gas velocity causing a large RH gradient which in turn causes a resistance gradient in the membrane. The large RH and resistance gradients explain why there are such large current gradients in the second half of the cell.

To maximize the diffusion in a fuel cell, it is necessary to reduce the velocity of the gas streams and minimize the mean free-diffusion path. The STR fuel cell achieves this by moving away from the channel to an open plenum design, where the only barriers to diffusion are the posts that are mandated for current collection. Fig. 8 compares the two fuel cell designs, assuming an air flow rate of 300 cm^3 min^{-1}, and demonstrates pictorially how the STR fuel cell improves back diffusion by reducing the gas velocity and reducing the mean free path that a molecule must travel to back-diffuse from point A to B. By reducing the gas velocity and mean free diffusion path, water molecules formed toward the exit can diffuse toward the entrance and are not convected away. It is for this reason that there is only a minimal depleted performance zone at the entrance (Fig. 5(a)) and why the overall current gradients are significantly less severe than in the serpentine fuel cell. Consequently, there is also an overall
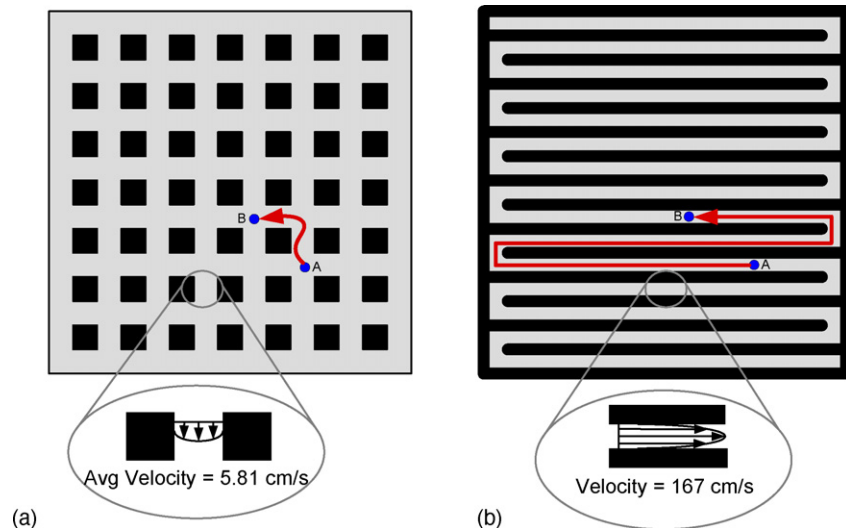

Fig. 8. Diagram showing velocity profile and mean free diffusion path in (a) STR fuel cell and (b) single-channel serpentine system.

Table 2
Comparison of characteristic diffusion velocity and characteristic convective velocity in STR and serpentine flow-fields

Flow design	Volume, V (cm³)	V/Q (s)	$(D/(V/Q))^{1/2}$ (cm s^{-1})	Effective A_c (cm²)	Q/A_c (cm s^{-1})	$(D/(V/Q))^{1/2}$: (Q/A_c)
STR	3.2	0.64	0.57	1.0	5	0.64
Serpentine	2.03	0.41	0.72	0.03	167	0.012

performance boost. It must also be noted that the design does not suffer a performance penalty under humidified conditions, as shown in Fig. 4.

Mathematically, it is possible to evaluate how well the serpentine and STR fuel cell systems are optimized to promote back-mixing through diffusion by comparing the characteristic diffusion velocity $(D/\tau)^{1/2}$ and characteristic convective velocity (Q/A_c) of the two systems, where: the residence time, τ, is equal to V/Q; the volume, V, is in cm³; Q is flow rate in cm³ s^{-1}; A_c is the cross-sectional area of the flow channel in cm²; D is the self-diffusivity of the gas in cm² s^{-1}. These two characteristic values for each of the flow field designs are given in Table 2. The data clearly show that the STR fuel cell has a significantly lower convective velocity. The ratio of the diffusive velocity to the convective velocity for the STR fuel cell design is over 50 times greater than for the serpentine fuel cell system. The large decrease in the convective velocity is responsible for the significantly improved back-mixing capability of the STR fuel cell design. Note: in all calculations the total flow rate of air was 300 cm³ min^{-1} and a diffusivity of 0.21 cm² s^{-1} was used. The calculations represent an approximation as they do not take into account changes in concentration and flow rate as the gases are consumed in the fuel cell.

The effect of having good diffusive back-mixing can be explained by considering the segmented fuel cell represented as a series of small fuel cells in parallel, as shown in Fig. 9(a) [9]. Using the circuit diagram model, it is possible to relate

the current output of a fuel cell to the internal resistance (R_{int}), external load resistance (R_L) and an ideal battery voltage (V_b), as represented by Eq. (1) where $\Im$ is Faraday's constant. The value of V_b can be calculated using the Nernst equation, (Eq. (2)) as a function of the ideal chemical potentials, α_i, of the gas phases and the activity of water, α_w.

$$i = \frac{V_b}{R_L + R_{int}} \quad (1)$$

$$V_b = \frac{-\Delta G^\circ}{2\Im} - \frac{RT}{2\Im} \ln \left(\frac{\alpha_{H_2}^{anode} (\alpha_{O_2}^{cathode})^{1/2}}{\alpha_{water}^{cathode}} \right) \quad (2)$$

When a fuel cell is operated with a single-channel serpentine configuration with dry feeds and low stoichiometry to reduce convection, the concentration of reactant gases will be highest at the entrance (FC1 in Fig. 9(a)), which means, that V_b is at a maximum (typically 0.9 V for a hydrogen/air fuel cell at 1 atm.). On the other hand, the internal resistance of the membrane will be high as there is no water in the feed stream and only minimal water production. This gives rises to a current–potential I–V plot with a steep slope, as seen in Fig. 9(b). Alternately, at the exit of the fuel cell (FC9 in Fig. 9(a)), the reactant concentration in the flow streams will be significantly depleted and will reduce the open-circuit voltage, V_b. The latter is compensated by a significant reduction in the internal resistance of the membrane (Fig. 9(c)). As shown by Eq. (1), a small change in the internal
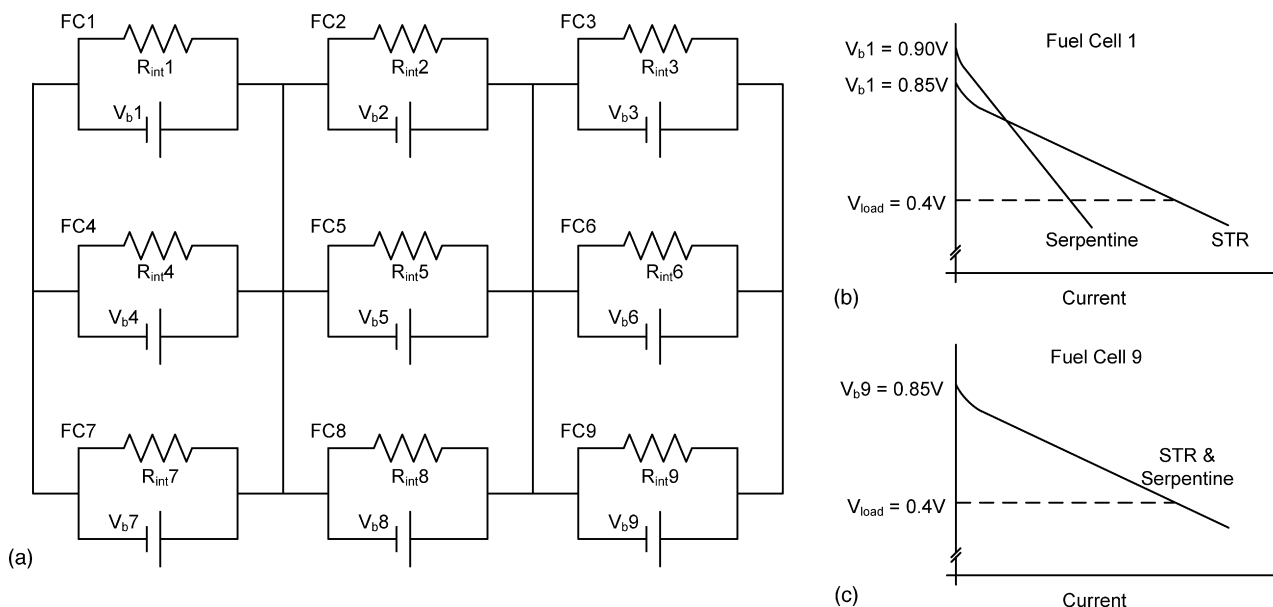

Fig. 9. (a) Circuit diagram representation of 3 × 3 segmented fuel cell; (b) representative dry feed I–V performance curve of FC1 (entrance) when operating in STR and serpentine modes; (c) representative dry feed I–V performance curve of FC9 (exit) when operating in STR and serpentine modes.

resistance of the membrane can have a large direct affect on the performance of the cell, whereas, as indicated by Eq. (2), an order of magnitude change in the reactant concentration at the cathode only reduces the open-circuit voltage by approximately 70 mV.

When considering an ideal, well-mixed, STR fuel cell operating under the same conditions, the concentration of the reactant gases will be uniform throughout the cell and equal to that at the exit. This causes a small reduction in the open-circuit voltage throughout the cell. The back-mixing which causes the uniform concentration also helps to ensure that the RH in the cell is at a maximum throughout the cell, thereby reducing the internal resistance. Hence, the I–V curve should be similar throughout the cell, as demonstrated in Fig. 9(b) and (c).

In a real world situation, it is not possible to have perfect mixing, but it is possible to design and optimize fuel cell systems to take advantage of the high diffusivity of the gas streams and the water that is created internally. The STR fuel cell design achieves this goal, and as a result performs better than single-channel serpentine flow designs.

5. Conclusions

The STR fuel cell exhibits superior overall performance and lower current, impedance and temperature distribution gradients than a single-channel serpentine fuel cell when operated with reduced RH feed streams. This is because the STR fuel cell has lower RH gradients in the fuel cell flow channels. Low RH gradients are achieved by controlling the operating parameters and optimizing the flow-field design. The optimized STR flow-field design employs an open-channel design which reduces the gas velocity and mean free diffusion path. By reducing these parameters, water can more easily back-diffuse towards the feed inlet. Controlling water convection through regulation of feed flow rates allows the STR fuel cell to perform optimally. The test equipment with the segmented test cell enables spatially-resolved characterization of different flow fields.

Acknowledgements

References

[1] M. Fronk, Ninth Grove Fuel Cell Symposium, Elsevier, London, UK, 2005.
[2] A. Martin, Ninth Grove Fuel Cell symposium, Elsevier, London, UK, 2005.
[3] M. Oszcipok, M. Zedda, J. Hesselmann, M. Huppmann, M. Wodrich, M. Junghardt, C. Hebling, J. Power Sources 157 (2) (2006) 666–673.
[4] W. Hogarth, J. Benziger, J. Power Sources 159 (2) (2006) 968–978.
[5] J. Benziger, E. Chia, E. Karnas, J. Moxley, C. Teuscher, I.G. Kevrekidis, J. AIChE 50 (8) (2004) 1889–1900.
[6] W. Hogarth, J. Benziger, J. Electrochem. Soc. 153 (11) (2006) A2139–A2146.
[7] A. Hakenjos, H. Muenter, U. Wittstadt, C. Hebling, J. Power Sources 131 (1/2) (2004) 213–216.
[8] A. Hakenjos, C. Hebling, J. Power Sources 145 (2) (2005) 307–311.
[9] J. Benziger, M. Satterfield, W. Hogarth, J. Nehlsen, I. Kevrekidis, J. Power Sources 155 (2) (2006) 272–285.